THE FLY'S EYE: STATUS & FUTURE PROSPECTS

R. Cady, G. L. Cassiday, J. Elbert, E. Loh,
P. Sokolsky, D. Steck, M. Ye
University of Utah, Salt Lake City, UT 84112

ABSTRACT

We describe a high energy physics observatory, the Fly's Eye, designed to measure extensive air showers (EAS) in the energy range 10^{17}-10^{21}eV via atmospheric fluorescence. Preliminary results are presented for the following measurements: (1) the high energy cosmic ray spectrum, at 10^{17}-10^{19}eV, (2) the total proton cross section σ_{pp}, (3) limits on the extra-galactic neutrino flux at 10^{20}eV.

INTRODUCTION

The "Fly's Eye" (see Fig. 1) is a high energy physics/astrophysics observatory designed to detect ultrahigh energy cosmic rays (UHCR; $E \gtrsim 10^{17}$eV) via air fluorescence. It consists of two stations separated by 3.3Km. The 1st station (Fly's Eye I) consists of 67 62-inch mirrors, 880 associated photomultipliers and Winston light collecting funnels arranged in clusters of 12 or 14 tubes mounted in the focal plane of each mirror. The second station, Fly's Eye II, is smaller, consisting of only eight mirrors and associated PMT clusters. Fly's Eye I is designed to image the entire night sky (2π steradians) and thus to detect the passage of EAS thru the atmosphere generated by an incoming UHCR cosmic ray primary. Even though the

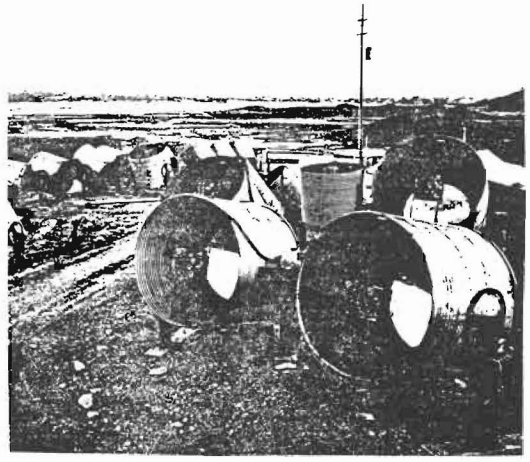

Fig. 1. Schematic of Fly's Eye. Incoming cosmic ray generates EAS viewed optically by an array of 67 mirrors and 880 PMT's.

atmosphere is a poor scintillator ($\lesssim$ 0.1% efficiency; see Fig. 2 and 3), the overwhelming amount of energy being liberated by the large number of charged particles in an EAS ($n \sim 10^{7}$-10^{12}) makes it possible to optically detect cosmic rays with energies exceeding 10^{20}eV out to distances of the order of 20Km or so. Experimental measurements to be carried out with this detector include the following:

(1) $\sigma_{p_{air}}$
(2) Secondary multiplicity growth.
(3) Search for rare but potentially exciting events, i.e., "Centauros".
(4) Detect or place spectrum limits on the extra-galactic neutrino flux.
(5) Composition of cosmic ray primaries.
(6) Cosmic ray spectrum.
(7) Cosmic ray anisotropies.
(8) Search for high energy UHCR spectrum cut-off.[1]

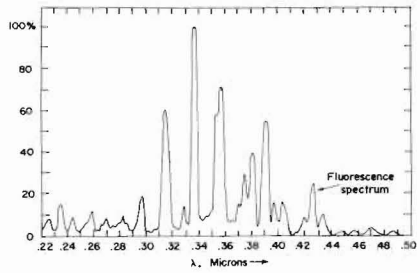

Fig. 2. Atmospheric fluorescence

The physics listed above constitute a unique blend of high energy particle physics and astrophysics. No previous experimental program initiated to investigate the behavior of UHCR has completely succeeded in disentangling the effects of particle physics (i.e., cross section & multiplicity) from those of astrophysics (composition). This situation arises from the hitherto unsolved difficulty of obtaining both good count rate and resolution. The Fly's Eye detector represents an attempt to overcome this limitation in the UHCR regime. Relevent detector parameters are listed in Table I.

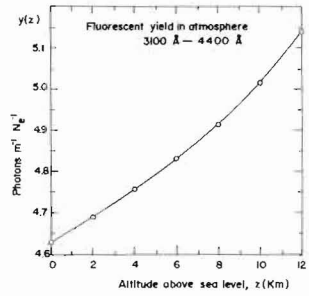

Fig. 3. Photon yield/m/electron vs. atmospheric altitude.

The low UHCR intensity constitutes a formidable problem for the experimentalist. Shown in Fig. 4 is a luminosity vs. energy diagram for a large number of existing or proposed accelerators. Also shown for comparison is the region of luminosity-energy accessible to the Fly's Eye. It is clear from such a plot that the low luminosity limits such a detector to the study of processes with cross sections at the millibarn level. However, the Fly's Eye detector alone occupies the energy regime $10^{4}\text{GeV} \lesssim S^{1/2} \lesssim 10^{6}\text{GeV}$ and this situation is likely to persist for a long time to come. Fortunately, the "beam" is free and one can counteract, somewhat, the low Fly's Eye luminosity by spending a long time taking data in order to obtain reasonably accurate cross section/multiplicity measurements. Long observation time is necessary anyway in order to carry out the specified UHCR astrophysics experiments.

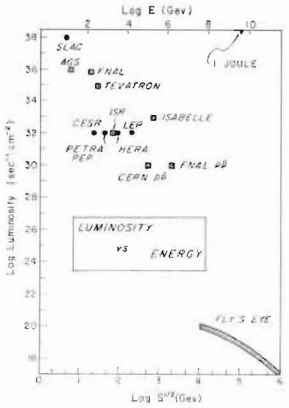

Fig. 4. Luminosity vs Energy

TABLE 1
Fly's Eye Parameters

		FE I	FE II
1.	# of Mirrors	67	8
2.	Diameter	1.6 meters	
3.	focal length	1.5 meters	
4.	Obscuration	~ 13%	
5.	Aberration	~ 20mrad	
6.	# PMT & (Winston Cones)	880	112
7.	PMT efficiency (EMI 9861B)	20%	
8.	Mirror/Winston Cone Reflectivity	85%	
9.	Overall light gathering ε	65%	
10.	Angular field of view/PMT	5°	
11.	#Electronics Analog Channels	3520	448
12.	Charge dynamic range	~ 10^5 (linear)	
13.	Time resolution	± 25nsec	
14.	Angular resolution	± 1°	

EVENT RECONSTRUCTION & SHOWER SIZE ANALYSIS.

Shown in Fig. 5 is a schematic of the geometry of an EAS as seen by the Fly's Eye. The location of the EAS track in space can be obtained by measuring four parameters: two parameters determine the plane in which the EAS lies while two additional parameters (R_p - the impact parameter and ψ - the ground impact angle) determine the orientation of the track in that plane. The plane can be obtained purely from geometry of hit PMT's (see Fig. 6) while the other two parameters can be obtained from accurate timing given the kinematics of a light source propagating thru the sky at the speed of light. Consecutive PMT pulses arrive at the detector according to times given by the following expression $ct=ct_o + R_p \tan[(\chi_o - \chi)/2]$ (χ_o is the angle of shower observation at t_o, i.e., it represents the direction of shower approach; $\chi_o + \psi = \pi$).

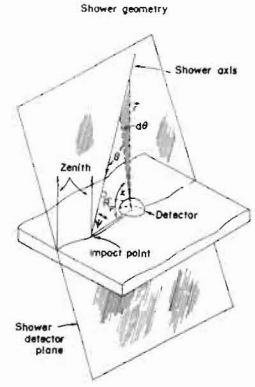

Fig. 5. Fly's Eye Shower Geometry

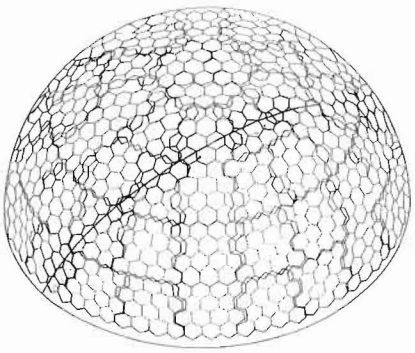

Fig. 6. Projection of Fly's Eye aperture onto "celestial" sphere. EAS track projects as a great circle.

Shown in Fig. 7 and 8 are the results of track reconstruction for a single event. In Fig. 7, the shower track has been projected onto the "celestial sphere", i.e., it represents the picture an observer would see looking up at a line source of light projected onto the night sky. Due overhead is the center of the dashed line curve which represents the horizon. Each hit PMT is indicacated by a number. Noise PMT's, (out of time and spatial sequence) are indicated by large X's. Small x's denote barely non-coplanar, small amplitude tubes that marginally triggered primarily due to scattered light or the diffuse edges of the EAS, itself. The numbers represent the time order of firing. Clearly, this event passed due overhead and disappeared out of aperture on the western horizon. Fig. 8 illustrates the timing sequence for this event (times have been converted to kilometers). The impact parameter for the event was 1.52 ± .02 Km while the zenith and azimuthal angles were 38.8 ± 1.3° and 353.6 ± 0.1° respectively.

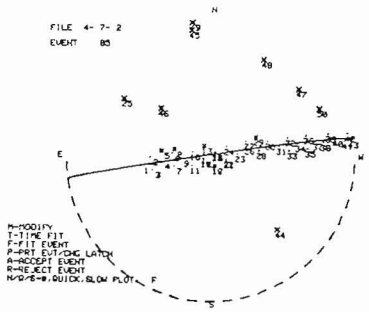

Fig. 7. Real Event progressing across Fly's Eye aperture, Fly's projected onto celestial sphere as seen by a ground observer. Numbers indicate PMT firing sequence. Large x indicates "noise" PMT's. Small x indicates, barely non-coplanar small amplitude PMT's.

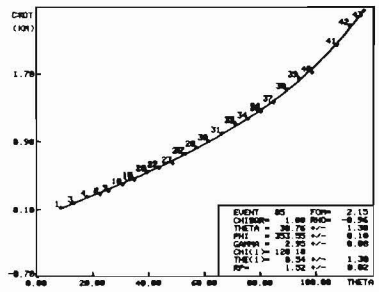

Fig. 8. Timing Curve ct vs θ, shower emission angle for event shown in Fig. 7. Best fit values shown in insert.

Given the geometry of the event one can now use the recorded pulse integrals to convert the light yield received at the detector into shower size N_e as a function of distance along the shower's trajectory. Furthermore, given the atmospheric scintillation efficiency, one can then calculate the number of charged particles in the shower which generated that light. The photoelectron yield obtained by each hit PMT is: $N_{pe} = N_e Y \frac{\varepsilon A}{4\pi R^2} \exp(-R/\lambda)\Delta\ell$

where

N_e = shower size at observed location along trajectory
Y = fluorescent light yield (~ 5 photons/m/electron) (see Fig. 3)
ε = combined light collection efficiency and photoelectron conversion efficiency (~0.17 ± 20%)
A = effective light gathering area (1.7m^2)
λ = attenuation length of 3600Å photons in air (~18Km)
R = distance of EAS to detector
$\Delta\ell$ = differential shower path length in field of view $\Delta\theta$ (Figure 5) since $\Delta\ell = \Delta(R_p/\tan\theta) = R_p\,\Delta\theta/\sin^2\theta$ we have:

$$N_e = \frac{4\pi}{Y\Delta\theta}\,\frac{1}{\varepsilon A}\,R_p\,N_{pe}\exp(R/\lambda)$$

Shower size measurements are weakly dependent on angle except for angles less than 20-30° where Cherenkov light begins to dominate scintillation light. For angles larger than 30° shower sizes have been determined to ~±20%. Ultimately, we believe we can obtain ~±5% accuracy with improved calibration.

Shown in Fig. 9 is the result of applying the above analysis to event 85. Shower sizes as a function of observation angle have been coverted to size vs atmospheric penetration "slant" depth in gm cm^{-2}

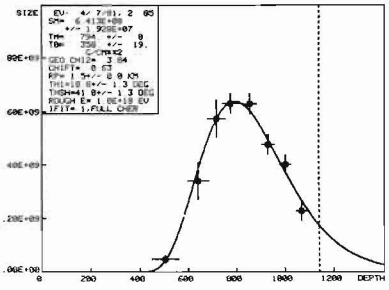

Fig. 9. Result shower size vs. atmospheric slant depth. Dotted line indicates earth surface. "0" depth at top of atmosphere. Shower energy about 10^{18}eV.

along the shower's trajectory. Overlapping angular intervals are binned and averaged in order to obtain this curve. The solid line is the result of fitting the data with the Gaisser-Hillas parameterization of shower development given by the expression:[2]

$$N(E_o, X) = N_o \frac{E_o}{\varepsilon} \exp^p\left(\frac{x-x_o}{X_{max}-\lambda}\right)^p \exp(-(x-x_o)/\lambda)$$

Where E_o = shower energy, x_o = location of 1st interaction
X_{max} = location of shower maximum

N_o = .045, ε = .074 GeV, λ = 70 g/cm^2, $p = (X_{max}-\lambda)/\lambda$

Due to its penetrating nature (X_o ~ 358g cm^{-2}; X_{max} ≃ 794g cm^{-2}) this particular event appears to have been generated by a proton whose energy was about 10^{18}eV! We would anticipate that an incoming iron nucleus, for example, would not have been so penetrating. By judiciously selecting such events we can insure a proton-enriched sample and then by plotting the distribution of event maxima we can estimate the proton-air interaction length and hence the pp inelastic cross section. This procedure is carried out in the last section.

CHECKS ON ANALYSIS

In order to insure that trajectories have been properly measured (depth perception with a single eye is difficult) and that recorded pulse integrals accurately reflect light yields, we have built and calibrated a high intensity pulsed xenon flasher permanently installed at Fly's Eye II and periodically fired over and above Fly's Eye I. This high intensity light pulse propagates up and out of the atmosphere and the scattered light it generates along the way (Rayleigh and Mie scattering) is picked up by the detectors at Fly's Eye I. Thus, the event sequence strongly resembles an inverse EAS. By analyzing the received signals in the same way as for real events we can calculate both trajectories and light yields and in this case compare them to known values in order to assess the accuracy of track reconstruction and size analysis. Fig. 10 represents a summary of analysis of 32 "flasher" events.

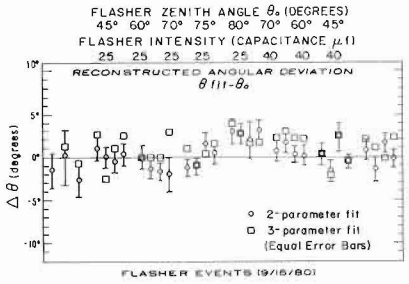

Fig. 10. Angular difference between best fit zenith angle and known zenith angle for 32 "flashergenerated" events. Observed deviations indicate angular accuries ~±2°.

We have also purchased and installed a pulsed nitrogen laser in order to generate much more accurate trajectories than could be generated with the xenon flasher. The laser generates a much shorter (100 psec) and better collimated (5m rad) light pulse than that of the xenon flasher (2-3 μsec, 50m rad). Indeed, shown in Fig. 11 is a timing curve for a trajectory

generated by the nitrogen laser. The zenith angle setting for the laser was 70°. The fitted value was 69.89° ± 1.3°! A systematic analysis of 300 such laser events yields a zenith angle error of ± 1.5° averaged over zenith and azimutal angles.

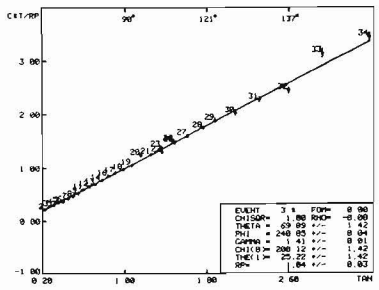

Fig. 11. Timing Curve cT_{R_p} vs TAN(θ/2) for laser generated event.

We show in Fig. 12, the result of shower "size" analysis applied to a single flasher event. No corrections were applied to the data. Each data point represents the conversion of the light received by a single PMT to the number of photons present in the propagating flasher beam. Conversion is based solely on track geometry and estimates of the Rayleigh and Mie scattered light received at the PMT. There were 10^{14} photons in the beam. Amplitude accuracy is about ± 20% as advertised. This result gives us confidence not only in our overall calibration but also in knowledge of how the atmosphere attenuates and scatters light!

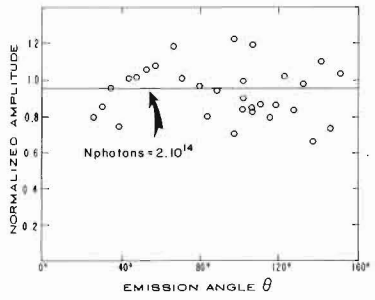

Fig. 12. Estimated # of photons in xenon flasher light pulse whose scattered light recorded by Fly's Eye PMT's. All pulse heights recorded over emission angles θ ranging from 20° -160° yield correct # of photons to ± 20%.

Approximately 15% of events seen by Fly's Eye I, will also be seen by FLy's Eye II. For these events, geometrical reconstruction is particularly simple, since the direction of the shower must lie along the intersection of the two planes defined by the two eyes. The additional timing information effectively allows us to do a 2-constraint fit to the trajectory. The subsample of events visible from both eyes will allow us to more fully understand both geometrical reconstruction systematics and our understanding of Cherenkov light contamination and propagation thru the atmosphere since the same part of an EAS will be viewed from two very different angles and distances. The second eye has become operational in September and further understanding of systematics awaits the accumulation of data with with both eyes.

RESULTS

The High Energy Cosmic Ray Spectrum. Shown in Fig.13

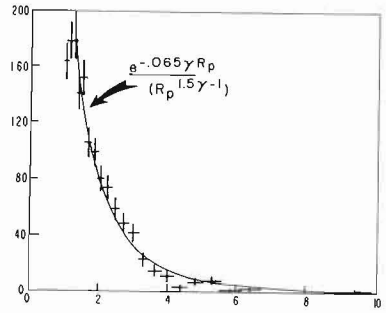

Fig. 13. Differential impact parameter distribution for about 1500 events. Best fit to observed falloff indicates integral energy spectral slop of γ~2.1±0.3.

is the differential impact parameter (R_p) distribution for a sample of about 1500 events. Measuring a shower's energy depends upon obtaining shower profiles over a rather long baseline. Until Cherenkov light contamination and residual reconstruction systematics are better understood, this procedure can be carried out only for a limited data sample at present. On the other hand, R_p can be precisely determined for a much larger data sample and since a shower's energy or, equivalently, its size is proportional to R_p, the R_p distribution should relate to the primary cosmic ray energy distribution. Quite simply we have $dN \propto I(>E) 2\pi R_p dR_p$ where $I(>E)$ is the integral primary cosmic ray spectrum. If $I(>E) \propto E^{-\gamma}$ and based upon the fact that Fly's Eye triggering electronics operates by preserving its signal to noise ratio over a wide dynamic time range, we estimate that

$$E \propto Ne \propto e^{\cdot 065 R_p (R_p^{1.5})}$$

Hence,

$$\frac{dN}{dR_p} \propto e^{-.065\gamma R_p / R_p(^{1.5\gamma-1})}.$$

In addition to this rather rough estimate of the spectrum, we are in the process of developing a Monte-Carlo program designed to completely simulate the response of the Fly's Eye to UHCR. We show in Figure 14 the resultant impact parameter distribution obtained from the Monte Carlo. The program was run by generating events at random whose energies were in excess of $2 \cdot 10^{17}$eV and stopping the run when the total number of event triggers was identical to that in real data sample. We find the best fit to the distribution shown in Fig. 13 yields a value of $\gamma = 2.0 \pm .1$ which is in agreement with the results of Watson,[4] for shower energies less than 10^{19}eV. Our data sample spans the energy range of 2.10^{17}eV - 5.10^{19}eV. Also note that the smallest Monte-Carlo event in the sample ($E=2 \cdot 10^{17}$eV) occurred at 1Km while the largest event $4 \cdot 10^{19}$eV occurred at ~10Km precisely as for the real data. Thus, we believe that our overall normalization is well-determined! Watson[4] reports a spectral flattening for cosmic rays with energies $>10^{19}$eV. Such a flattening would show up as an enhancement in our R_p distribution at impact parameters $R_p \gtrsim 4$-6Km. We see only the tiniest hint--statistically insignificant--of such a flattening. However, the data reported here was obtained with the Fly's Eye "electronically cut-off" at $R_p \gtrsim 5$-8 Km or so

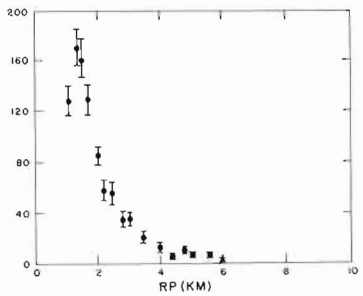

Fig. 14. Monte-Carlo generated impact parameter distribution. Normalized to total # event triggers. Compare with Fig. 13.

(the cut-off is geometry dependent). This cut-off was instituted in order to optimize the nearby lower energy event rate. Currently, we are "electronically tuned" to greater distances with the obvious goal of examing the quoted spectral flattening at $E \gtrsim 10^{19}$eV. Certainly, our preliminary spectral measurements for $E \gtrsim 10^{19}$eV are consistent with those obtained by other workers.

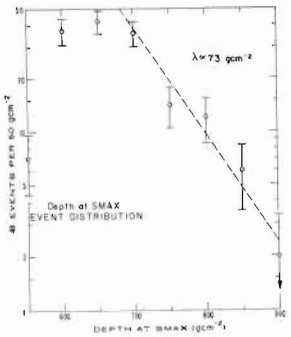

Fig. 15. Differential distribution of 90 events (at $E \sim 10^{18}$)vs. depth of shower Attentuation slope $\Lambda \sim 73$g cm^{-2} implies $\sigma^{tot}_{pp} \sim 120$mb.

Measurement of σ_{pp}. In Fig. 15 we show the distribution of shower maxima vs depth of maximum for a select sample of about 90 events with energies near 10^9GeV($S^{1/2} \sim 4 \cdot 10^4$GeV). The event sample was selected by demanding that the estimated error in shower maximum location be within $\pm$ 50 g cm^{-2}. The slope of this distribution (Λ_m) at large shower depths should relate to the nucleon-air interaction length λ_n. This relationship has been investigated in detail by Gaisser et al[5]. They conclude that: $\Lambda_m \sim 1.6\lambda_n$ and that the distribution of shower maxima is, in fact, as sensitive to the value of λ_n as is the distribution of even "earlier" observed points along the shower profile such as $\Lambda_{1/4}$ max. Furthermore, we should note that the slope of this distribution at large depths should be determined preferentially by protons as opposed to heavier cosmic ray primaries since protons presumably would be more penetrating on the average. We note that our measured slope $\Lambda_m \sim 73$g cm^{-2} implies a nucleon interaction length of $\lambda_n \sim 48$g cm^{-2} or $\sigma_{p\text{-air}} \simeq 500$mb and if Glauber theory[6] is used to estimate σ_{pp}, we obtain $\sigma^{tot}_{pp} \simeq 120$mb. This value lies between that obtained by a ln$s$ and ln$^2 s$ extrapolation.[5] (We quote no errors yet since we believe that the previously alluded

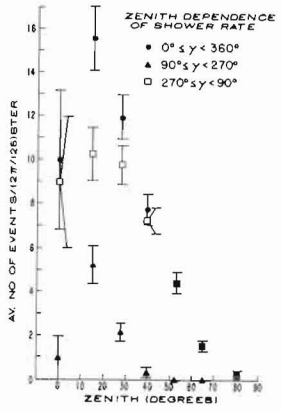

Fig.16. Zenith angle event distribution for about 600 showers with energies $>10^{18}$eV. γ-angle intervals refer to showers impacting either behing or in front of Fly's Eye.

to systematic difficulties may outweigh statistical problems.) Such a value for the cross section implies that a significant fraction of the cosmic rays contained in this data sample are protons. (If they were mostly Fe nuclei-their behavior is quite remarkable; however the presence of lighter nuclei, such as alphas, can certainly not be ruled out.) We point out that inaccuracies in locating the depth at maximum would probably decrease our estimated value of Λ_m. Hence, our estimate of σ^{tot}_{pp} probably represents a lower limit. Clearly, a larger number of more accurately measured events is necessary to (1) more accurately determine Λ_m and (2) look for changes in Λ_m indicative of compositional effects. A final value for σ_{pp} may await data taken with both Fly's Eye operational.

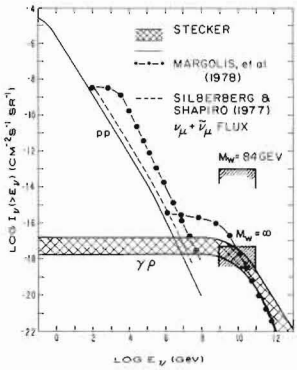

Fig. 17. Estimated limits on extragalactic neutrino flux near $E \sim 10^{20}$eV given $84\text{GeV} \lesssim M_W \lesssim \infty$.

Extragalactic Neutrino Flux

A search for extragalactic neutrino flux ($E_\nu \sim 10^{20}$eV) is necessarily dependent on the value of the neutrino cross-section at these energies. We consider two limiting cases: $M_W=\infty$ (4 point interaction) and $M_W=84\text{GeV}/C^2$ (Weinberg-Salam choice). If $M_W=\infty$, the earth is opaque to neutrinos of this energy and we search for them by looking for events with zenith angles between 80°-90°(the atmosphere is > 5000gm cm^{-2} so that hadrons will not penetrate into the fiducial volume). Fig. 16 shows the zenith angular distribution of ~ 600 events obtained with 2/3 of Fly's Eye I operational for about 6 months. We see no events with $80° < \theta_z < 95°$ and set a limit on the

$\nu_\mu+\nu_e$ flux shown in Fig. 17 ($M_W=\infty$). If $M_W=84 GeV/C^2$, the earth is ~10% transmitter and we can search for neutrinos by looking for upward-going (flasher-like) events. The best sensitivity is achieved for the ν_e flux, since at these energies the Landau-Pomeranchuk-Migdal effect[7] is operative and gives a radiation length in earth of ~ 100m. The results for this assumption is also shown in Fig. 17 ($M_W=84 GeV/C^2$). These limits should improve by factors of 20-100 as the experiment progresses and more realistic acceptance calculations done. If and when the W boson will be found and its mass determined, more definitive limits on the extra-galactic flux can be set. We note that since the most obvious source of such high energy neutrinos is the interaction of the primary cosmic ray flux with the 3°K black body radiation, such measurements could, in principle, confirm the universality of the 3°K radiation in extragalactic space.

Future Prospects:

There is a two prong thrust to improve the Fly's Eye: noise reduction and spatial resolution improvement. To reduce the night sky background radiation from stars, planets and street lights, optical filters (UG-1) are being installed on 14 phototubes as a small scale test. We expect the filters will enable us to expand the visible volume of the detector as well as extend the observation time into nights when a small fraction of the moon is visible.

We are also designing a fine resolution Fly's Eye to supplement our existing detectors. Optimization of the design based on our experience with the existing eye and new phototubes and electronics has begun this summer. The high resolution eye will enable us to extend the visible fiducial area beyond our present radius as well as give us improved shower profile measurement.

Whether we will proceed to fully instrument the second eye, develop a single high resolution eye, or both, will depend to a large extent on understanding the data which we will take with both eyes in the following year.

REFERENCES

1. K. Greisen, Phys. Rev. Let. 16, 748 (1966).
2. T. K. Gaisser and A. M. Hillas, 15th Int. Cosmic Ray Conf. 8. 353 (1977).
3. F. W. Stecker, NASA Tech. Memorandum 79609, GSFC, Greenbelt, MD. (1978).
4. A. A. Watson, 16th Moriond Astrophysics Meeting "Cosmology and Particles" Les Arcs, France, edited by J. Andouze et al, editions Frontieres March 15-21, 1981.
5. T. K. Gaisser (see proceedings--Madison Conference on High Energy Collider Physics, Dec. 1981.)
6. R. J. Glauber and G. Matthiae, Nucl. Phys. B21, 135 (1970).
7. E. Knoishi, et. al., Nuevo Cimento, 44A, 509 (1978)